Image-based modelling of ocean surface circulation from satellite acquisitions

Dominique Béréziat, Isabelle Herlin

Image-based modelling of ocean surface circulation from satellite acquisitions

Dominique Béréziat[1] and Isabelle Herlin[2,3]

Université Pierre et Marie Curie, 4 place Jussieu, Paris 750005, France

[2]*Inria, B.P. 105, 78153 Le Chesnay, France*

[3]*CEREA, joint laboratory ENPC - EDF R&D, Université Paris-Est, Cité Descartes Champs-sur-Marne, 77455 Marne la Vallée Cedex 2, France*

Dominique.Bereziat@upmc.fr, Isabelle.Herlin@inria.fr

Abstract: Satellite image sequences permit to visualise oceans' surface and their underlying dynamics. Processing these images is then of major interest in order to better understanding of the observed processes. As demonstrated by state-of-the-art, image assimilation allows to retrieve surface motion from image sequences, based on assumptions on the dynamics. In this paper we demonstrate that a simple heuristics, such as the Lagrangian constancy of velocity, can be used, and successfully replaces the complex physical properties described by the Navier-Stokes equations, for assessing surface circulation from satellite images. A data assimilation method is proposed that includes an additional term $\mathbf{a}(t)$ to this Lagrangian constancy equation. That term summarises all physical processes other than advection. A cost function is designed, which quantifies discrepancy between satellite data and model values. The cost function is minimised by the BFGS solver with a dual method of data assimilation. The result is the motion field and the additional term $\mathbf{a}(t)$. This last component models the forces, other than advection, that contribute to surface circulation. The approach has been tested on Sea Surface Temperature of Black Sea. Results are given on four image sequences and compared with state-of-the-art methods.

1 INTRODUCTION

Satellite image sequences permit to visualise oceans' surface and their underlying dynamics. Processing these images is then of major interest in order to better understanding of the observed processes and forecast extreme events. As demonstrated by state-of-the-art, image assimilation allows to retrieve surface motion from image sequences, using heuristics on the dynamics (Papadakis et al., 2007; Titaud et al., 2010).

Advanced 3D oceanographic models are available in the literature. These models are based on Navier-Stokes equations (see for instance the NEMO model[1]). As satellites nowadays observe the sea surface with a high spatial resolution, it becomes possible to estimate surface circulation from these data with a simplified model, such as the shallow water model (Vallis, 2006). This 2D model has been proven to be suitable for representing the surface circulation of closed seas, such as Black Sea (Oguz et al., 1992). The shallow water equations have also been success-

fully used to estimate the upper layer circulation of Black Sea from Sea Surface Temperature (SST) images (Korotaev et al., 2008; Huot et al., 2010) with a data assimilation method.

In this paper, we propose to learn dynamics from SST image acquisitions with a data assimilation method applied to an empirical model, derived from the shallow water equations. This is an image-based approach to model the surface dynamics. In the shallow water model, surface circulation is described by the horizontal velocity, that is advected by itself and subject to geophysical forces such as Coriolis, Earth gravity and viscosity. The advection process is kept in the empirical model, but all non-transport components are summarised in a global term, denoted $\mathbf{a}$ (letter $\mathbf{a}$ stands for additional), that is estimated by our approach. Adding this term to the advection one is similar, from a mathematical point of view, to the weak data assimilation framework (Sasaki, 1970; Dee, 2005; Trémolet, 2006; Valur Hólm, 2008). Such data assimilation method is then designed to compute the solution: a cost function is constructed whose con-

---

[1] http://www.nemo-ocean.eu/

trol variables are the motion field at the first acquisition date and the value of the additional term $\mathbf{a}(t)$ at each date of the acquisition interval. The minimum of the cost function is obtained thanks to optimal control techniques (Lions, 1971).

Section 2 provides the notations that are used in the remaining of this paper and the mathematical description of the proposed approach in order to model the dynamics of the ocean's upper layer. The data assimilation method is briefly outlined in Section 3. It corresponds to a weak formulation with a non advective term in the evolution equation. The implementation is shortly given in Section 4, in order to permit that interested Readers apply the method by themselves. Results on four SST image sequences acquired over Black Sea by NOAA-AVHRR sensors are displayed and quantified in Section 5.

2 PROBLEM STATEMENT

Image data are acquired on a bounded rectangle of $\mathbb{R}^2$, named Ω, and on a temporal interval $[0,\mathrm{T}]$. Let define $A = \Omega \times [0,\mathrm{T}]$ the corresponding space-time domain, on which the dynamics is modelled. A point $\mathbf{x} \in \Omega$ is defined as $\mathbf{x} = \begin{pmatrix} x & y \end{pmatrix}^T$ and the motion vector at point $\mathbf{x}$ and date $t \in [0,\mathrm{T}]$ is written $\mathbf{w}(\mathbf{x},t) = \begin{pmatrix} u(\mathbf{x},t) & v(\mathbf{x},t) \end{pmatrix}^T$. At each date t, the motion field on the domain Ω is written as $\mathbf{w}(t)$. N Sea Surface temperature acquisitions are available at dates t_i, $i = 1 \cdots N$. They are denoted $T(t_i)$ with pixels values $T(\mathbf{x},t_i)$.

A state vector $\mathbf{X}$ is defined on A. It includes the two components u and v of the motion vector $\mathbf{w}(\mathbf{x},t)$ and a pseudo-temperature value $T_s(\mathbf{x},t)$, which has properties similar to those of the Sea Surface Temperature value: $\mathbf{X}(\mathbf{x},t) = \begin{pmatrix} \mathbf{w}(\mathbf{x},t)^T & T_s(\mathbf{x},t) \end{pmatrix}^T$. At the end of the data assimilation process, the discrepancy between the pseudo-temperature and the satellite acquisition values has to be small.

The heuristics on dynamics, used in the paper, are derived from the shallow water equations, that express the principles of mass and momentum conservation. Circulation of the upper ocean is represented by the 2D velocity $\mathbf{w} = \begin{pmatrix} u & v \end{pmatrix}^T$ and the thickness h of the mixed layer. The sea surface temperature T_s is transported by the motion field. This provides the set of equations:

$$\frac{\partial u}{\partial t} = -u\frac{\partial u}{\partial x} - v\frac{\partial u}{\partial y} + fv - g'\frac{\partial \eta}{\partial x} + K_{\mathbf{w}}\Delta u \quad (1)$$

$$\frac{\partial v}{\partial t} = -u\frac{\partial v}{\partial x} - v\frac{\partial v}{\partial y} - fu - g'\frac{\partial \eta}{\partial y} + K_{\mathbf{w}}\Delta v \quad (2)$$

$$\frac{\partial \eta}{\partial t} = -\frac{\partial(u\eta)}{\partial x} - \frac{\partial(v\eta)}{\partial y} - h_m\left(\frac{\partial u}{\partial x} + \frac{\partial v}{\partial y}\right) \quad (3)$$

$$\frac{\partial T_s}{\partial t} = -u\frac{\partial T_s}{\partial x} - v\frac{\partial T_s}{\partial y} + K_T\Delta T_s \quad (4)$$

with η the thickness anomaly $\eta = h - h_m$, h_m the average value of h, K_T the temperature diffusion parameter, f the Coriolis parameter, $K_{\mathbf{w}}$ the viscosity and $g' = g(\rho_0 - \rho_1)/\rho_0$ the reduced gravity. ρ_0 corresponds to the reference density and ρ_1 to the average density of the mixed layer.

As explained in the introduction, we propose to group all geophysical forces that do not correspond to advection in a unique term, named "additional term" and denoted by $\mathbf{a}$. The variable η is then considered as an hidden variable of the system and is included in $\mathbf{a}$. In such way, Eqs. (1),(2),(3) reduce to:

$$\frac{\partial u}{\partial t} = -u\frac{\partial u}{\partial x} - v\frac{\partial u}{\partial y} + a_u \quad (5)$$

$$\frac{\partial v}{\partial t} = -u\frac{\partial v}{\partial x} - v\frac{\partial v}{\partial y} + a_v \quad (6)$$

where $\mathbf{a} = \begin{pmatrix} a_u & a_v \end{pmatrix}$ expresses the discrepancy to the Lagrangian constancy of velocity:

$$\frac{d\mathbf{w}}{dt} = \frac{\partial \mathbf{w}}{\partial t} + (\mathbf{w}.\nabla)\mathbf{w} = \mathbf{a} \quad (7)$$

From Equations (1,2), we get:

$$a_u = fv - g'\frac{\partial \eta}{\partial x} + K_{\mathbf{w}}\Delta u \quad (8)$$

$$a_v = -fu - g'\frac{\partial \eta}{\partial y} + K_{\mathbf{w}}\Delta v \quad (9)$$

where η verifies Eq.(3).

Our approach allows to estimate $\mathbf{w}(0)$ and the additional term $\mathbf{a}(t)$ at each date $t \in [0,\mathrm{T}]$, thanks to a data assimilation process summarised in Section 3. Deriving the values $\mathbf{a}(t)$ allows to describe empirically the physical processes producing the image sequence.

Eqs. (7) and (4) are further contracted in an evolution model $\mathbb{M}$ of the state vector $\mathbf{X}$:

$$\frac{\partial \mathbf{X}}{\partial t} + \mathbb{M}(\mathbf{X}) = \begin{pmatrix} \mathbf{a} \\ 0 \end{pmatrix} \quad (10)$$

An observation equation links the state vector to the observed Sea Surface Temperature images acquisitions T:

$$\mathbb{H}\mathbf{X} = T + \varepsilon_R \quad (11)$$

The observation operator $\mathbb{H}$ projects the state vector into the space of image observations and consequently: $\mathbb{H}\mathbf{X} = T_s$. The term $\varepsilon_R(\mathbf{x},t)$ models the acquisition noise and the uncertainty on the state vector value. This last comes from the approximation of the model and from the discretization errors.

Some approximate knowledge of the value $\mathbf{X}(0)$ could be available and named background $\mathbf{X}_b$. However, the result of the state vector at date 0 is not exactly equal to that background value and a term ε_B is therefore introduced:

$$\mathbf{X}(\mathbf{x},0) = \mathbf{X}_b(\mathbf{x}) + \varepsilon_B(\mathbf{x}) \qquad (12)$$

The variables ε_R and ε_B are supposed independent, unbiased, Gaussian and characterised by their respective covariance matrices R and B.

Eqs. (10), (11), (12) summarise the whole knowledge that is available to model the surface dynamics. This knowledge is processed by our approach thanks to a data assimilation algorithm that is shortly described in Section 3.

3 DATA ASSIMILATION

In the data assimilation scientific community, an approach named weak 4D-Var has been defined: in order to obtain the solution $\mathbf{X}$ that solves System (10), (11), (12), a cost function is designed, that is minimised with control on ε_B and on the values of the additional term $\mathbf{a}$:

$$J[\varepsilon_B,\mathbf{a}] = \left\langle \varepsilon_B, B^{-1}\varepsilon_B \right\rangle + \int_t \gamma \|\nabla \mathbf{a}(t)\|^2$$
$$+ \int_t \left\langle \mathbb{H}\mathbf{X}(t) - T(t), R^{-1}(\mathbb{H}\mathbf{X}(t) - T(t)) \right\rangle \qquad (13)$$

where $\langle \cdot, \cdot \rangle$ denotes the canonical inner product in an abstract Hilbert space on which the state vector is defined, with norm $\|.\|^2$ and $\|\nabla \mathbf{a}\|^2 = \langle \nabla a_u, \nabla a_u \rangle + \langle \nabla a_v, \nabla a_v \rangle$.

The first term comes from Eq. (12) and expresses that the value $\mathbf{X}(0)$ at date 0 should stay close to the background value $\mathbf{X}_b$. The second term constrains the additional term $\mathbf{a}(t)$ to be spatially smooth. The last term, coming from Eq. (11), expresses that the pseudo-temperature value T_s has to be close to that of satellite acquisitions at the end of the assimilation process.

The gradient of J is derived with calculus of variation (Lions, 1971). Its two components are:

$$\frac{\partial J}{\partial \varepsilon_B}[\varepsilon_B,\mathbf{a}] = 2\left(B^{-1}\varepsilon_B + \lambda(0)\right) \qquad (14)$$

$$\frac{\partial J}{\partial \mathbf{a}(t)}[\varepsilon_B,\mathbf{a}] = 2\left(-\gamma\Delta\mathbf{a}(t) + \lambda(t)\right) \qquad (15)$$

with $\lambda(t)$ being the adjoint variable, that is computed backward with the two following equations:

$$\lambda(\mathrm{T}) = 0 \qquad (16a)$$

$$-\frac{\partial\lambda}{\partial t} + \left(\frac{\partial\mathbb{M}}{\partial\mathbf{X}}\right)^* \lambda = \mathbb{H}^T R^{-1}(\mathbb{H}\mathbf{X} - T) \quad (16b)$$

The adjoint operator $\left(\frac{\partial\mathbb{M}}{\partial\mathbf{X}}\right)^*$ is defined by:

$$\langle Z\eta, \lambda \rangle = \langle \eta, Z^*\lambda \rangle. \qquad (17)$$

Proof: For sake of simplicity, we suppose in this proof that Eq. (10) is written as $\frac{\partial\mathbf{X}}{\partial t} + \mathbb{M}(\mathbf{X}) = \mathbf{a}$.

The state vector and the functional J depend on ε_B and $\mathbf{a}(t)$. Let δJ and $\delta\mathbf{X}$ be the perturbations on J and $\mathbf{X}$ obtained if ε_B and $\mathbf{a}(t)$ are respectively perturbed by $\delta\varepsilon_B$ and $\delta\mathbf{a}(t)$.

From the definition of δJ, we obtain:

$$\delta J = 2\left\langle \delta\varepsilon_B, B^{-1}\varepsilon_B \right\rangle + 2\int_t \left(\gamma\langle\nabla\delta\mathbf{a}(t), \nabla\mathbf{a}(t)\rangle\right)$$
$$+ 2\int_t \left\langle \delta\mathbf{X}(t), \mathbb{H}^T R^{-1}[\mathbb{H}\mathbf{X}(t) - T(t)] \right\rangle \qquad (18)$$

The evolution equation of $\mathbf{X}$, Eq. (10), gives:

$$\frac{\partial\delta\mathbf{X}(t)}{\partial t} + \frac{\partial\mathbb{M}}{\partial\mathbf{X}}\delta\mathbf{X}(t) = \delta\mathbf{a}(t) \qquad (19)$$

and that of background, Eq. (12):

$$\delta\mathbf{X}(0) = \delta\varepsilon_B \qquad (20)$$

Eq. (19) gives, after multiplication by $\lambda(t)$ and integration on the space-time domain, the following equality:

$$\int_t \left\langle \frac{\partial\delta\mathbf{X}(t)}{\partial t}, \lambda(t) \right\rangle + \int_t \left\langle \frac{\partial\mathbb{M}}{\partial\mathbf{X}}\delta\mathbf{X}(t), \lambda(t) \right\rangle$$
$$= \int_t \langle \delta\mathbf{a}(t), \lambda(t) \rangle \qquad (21)$$

Integration by parts is applied on the first term and the adjoint operator is used in the second one in order to obtain:

$$\langle \delta\mathbf{X}(T), \lambda(T) \rangle - \langle \delta\mathbf{X}(0), \lambda(0) \rangle +$$
$$-\int_t \left\langle \delta\mathbf{X}(t), \frac{\partial\lambda(t)}{\partial t} \right\rangle + \int_t \left\langle \delta\mathbf{X}(t), \frac{\partial\mathbb{M}}{\partial\mathbf{X}}^* \lambda(t) \right\rangle \quad (22)$$
$$= \int_t \langle \delta\mathbf{a}(t), \lambda(t) \rangle$$

From Eq.(16a), it comes that $\langle \delta\mathbf{X}(T), \lambda(T) \rangle$ has a null value. From Eq. (20) it comes that $\langle \delta\mathbf{X}(0), \lambda(0) \rangle$ is equal to $\langle \delta\varepsilon_B, \lambda(0) \rangle$. Eq. (16b) is then used to obtain:

$$-\left\langle \delta\mathbf{X}(t), \frac{\partial\lambda(t)}{\partial t} \right\rangle + \left\langle \delta\mathbf{X}(t), \frac{\partial\mathbb{M}}{\partial\mathbf{X}}^* \lambda(t) \right\rangle = \qquad (23)$$
$$\left\langle \delta\mathbf{X}(t), \mathbb{H}^T R^{-1}(\mathbb{H}\mathbf{X}(t) - T(t)) \right\rangle$$

and rewrite Eq. (22) as:

$$\int_t \langle \delta\mathbf{X}(t), \mathbb{H}^T R^{-1}(\mathbb{H}\mathbf{X}(t) - T(t)) \rangle =$$
$$\langle \delta\varepsilon_B, \lambda(0) \rangle + \int_t \langle \delta\mathbf{a}(t), \lambda(t) \rangle \tag{24}$$

From this and Eq. (18), we derive:

$$\delta J = 2\langle \delta\varepsilon_B, B^{-1}\varepsilon_B \rangle - 2\int_t \gamma\langle \delta\mathbf{a}(t), \Delta\mathbf{a}(t)\rangle +$$
$$2\langle \delta\varepsilon_B, \lambda(0)\rangle + 2\int_t \langle \delta\mathbf{a}(t)\lambda(t)\rangle \tag{25}$$

and obtain the gradient of J, as written in Eqs. (14,15).

The cost function J is minimised with an iterative steepest descent method. At each iteration, the forward time integration of $\mathbf{X}$ is performed, according to Eq. (10). This forward integration provides the value of J. Then a backward integration of λ, according to Eqs. (16a) and (16b), computes the value of ∇J. An efficient solver (Byrd et al., 1995) is used to perform the optimisation given values of J and ∇J. (Le Dimet and Talagrand, 1986) is the first paper of the literature that describes the use of such method for estimating the initial state vector value.

4 NUMERICAL IMPLEMENTATION

Time integration of Eq. (10) relies on an explicit Euler scheme. Space discretization of motion advection:

$$\frac{\partial u}{\partial t} + u\frac{\partial u}{\partial x} + v\frac{\partial u}{\partial y} = 0 \tag{26}$$

$$\frac{\partial v}{\partial t} + u\frac{\partial v}{\partial x} + v\frac{\partial v}{\partial y} = 0 \tag{27}$$

involves a source splitting method (Wolke and Knoth, 2000), that is explained below.

Given an integration interval $[t_1, t_2]$, Eqs. (28) and (29) are first independently integrated:

$$\frac{\partial u^a}{\partial t} + u^a\frac{\partial u^a}{\partial x} = 0 \quad t \in [t_1, t_2] \tag{28}$$

$$\frac{\partial u^b}{\partial t} + v\frac{\partial u^b}{\partial y} = 0 \quad t \in [t_1, t_2] \tag{29}$$

with $u^a(x,y,t_1) = u^b(x,y,t_1) = u(x,y,t_1)$. Then $u(x,y,t_2)$ is obtained as $u(x,y,t_2) = u^b(x,y,t_2) + u^a(x,y,t_2) - u(x,y,t_1)$.

The linear advection of Eq. (29) is approximated by a first-order upwind scheme, as described in (Hundsdorfer and Spee, 1995). The nonlinear advection of Eq. (28) is first rewritten in a conservative form:

$$\frac{\partial u}{\partial t} + \frac{\partial}{\partial x}\left(\frac{1}{2}u^2\right) = 0 \tag{30}$$

and approximated by a first-order Godunov scheme (LeVeque, 1992).

The backward time integration of the adjoint variable λ involves the adjoint operator $\left(\frac{\partial \mathbb{M}}{\partial X}\right)^*$ (see Eq. (16b)). In order to be accurate, the method requires the adjoint of the discrete model and not the discretization of the continuous adjoint. The discrete adjoint operator $\left(\frac{\partial \mathbb{M}}{\partial X}\right)^*$ is then obtained with the automatic differentiation software Tapenade (Hascoët and Pascual, 2004; Hascoët and Pascual, 2013).

The background used in Eq. (12) is defined as null for motion and as the first image of the studied sequence for the pseudo-temperature.

5 RESULTS

For sake of simplicity, we name in the following EM, or Empirical Model, the dynamic model described in Sections 2 and 3: it includes the advection model and the additional term summarising the Coriolis, gravity and viscosity forces.

The proposed method has been experimented on several Sea Surface Temperature (SST) sequences, acquired over Black Sea by NOAA-AVHRR sensors, and results are given for four of them in this paper.

First, we discuss the ability of the proposed method to correctly estimate motion. For that purpose, EM results are compared with those obtained by one of the best optical flow method (Sun et al., 2010) of the literature. The satellite sequence is displayed on Figure 1. Acquisition dates are at 30 min, 6 hours, 15 hours, and 30 hours after the beginning of the studied temporal interval. Two gyres are clearly visible on these data. Motion results $\mathbf{w}(0)$, obtained by (Sun et al., 2010) and EM, are displayed on Figure 2. EM successes to capture the two gyre structures while Sun et al. fails. As $\mathbf{w}(0)$ is obtained from the analysis of the whole image sequence, its correct estimation means that the physical processes involved in $\mathbf{a}(t)$ are correctly assessed by the empirical model. It means that the geophysical non advective forces may be described as a whole in a unique term $\mathbf{a}(t)$.

Second, we examine the capability of EM to track features or points of interest on the whole image sequence. An accurate tracking result means that motion estimated by EM is correct on the studied temporal interval and properly transports image structures. A sequence of four SST images acquired in October 8th 2005 is displayed on Figure 3. Acquisition dates are at 30 min, 10 hours 15 min, 12 hours, 15 hours 30 min, after the beginning of the studied interval. Nine characteristic points are defined in white on the first
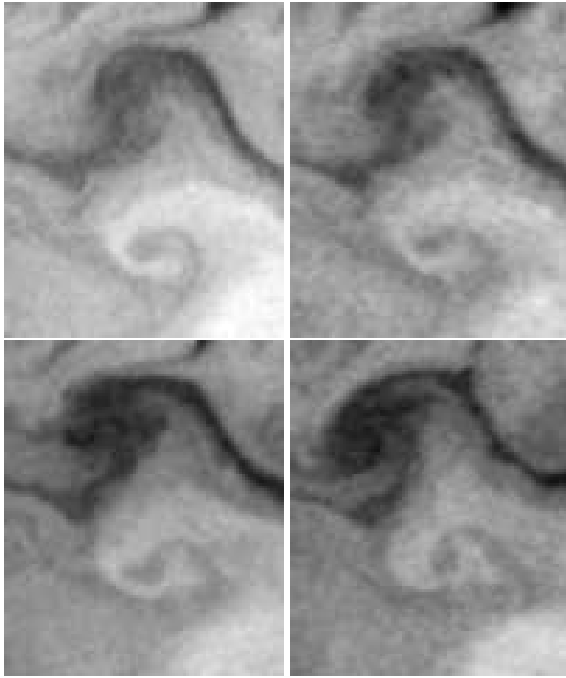
Figure 1: Top to bottom, left to right: SST images acquired on October 10th 2007, over Black Sea.

Figure 2: Motion results computed by Sun (up) and EM (down) at first observation date. The arrow representation is superposed to the coloured one.

observation. Points are surrounded by a coloured circle that helps to discriminate them on the following observations. These points are considered as characteristic, because they sample the various types of trajectories that can be observed on the sequence. On observations 2 to 4, the position of these nine points obtained with Sun's method are in red while those obtained with EM are in blue. On the fourth acquisition, in the "light pink circle" on the upper right, the point obtained with Sun's optical flow is outside of the image domain. Looking at the trajectories, it can be observed that Sun's algorithm fails to track these characteristic points, due to a wrong estimation of motion.

Another sequence of five SST images, acquired in July 2007 is displayed on Figure 4. Acquisition dates are at 30 min, 8 hours 15 min, 13 hours, 22 hours 30 min, 24 hours 30 min from the beginning of the studied interval. Seven characteristic points are defined in white on the first observation. Points positions obtained with Sun's optical flow are in red while those obtained with EM are in blue. At the second date, two points are at the same position with Sun's method and EM: only the red point is visible as the blue one is hidden behind it. On the fourth observation, one red point has disappeared as it is located outside of the image domain. On the last image, the colour of the ellipse surrounding each set of points gives an additional information on the quality of the result: a blue ellipse means that our method gives the
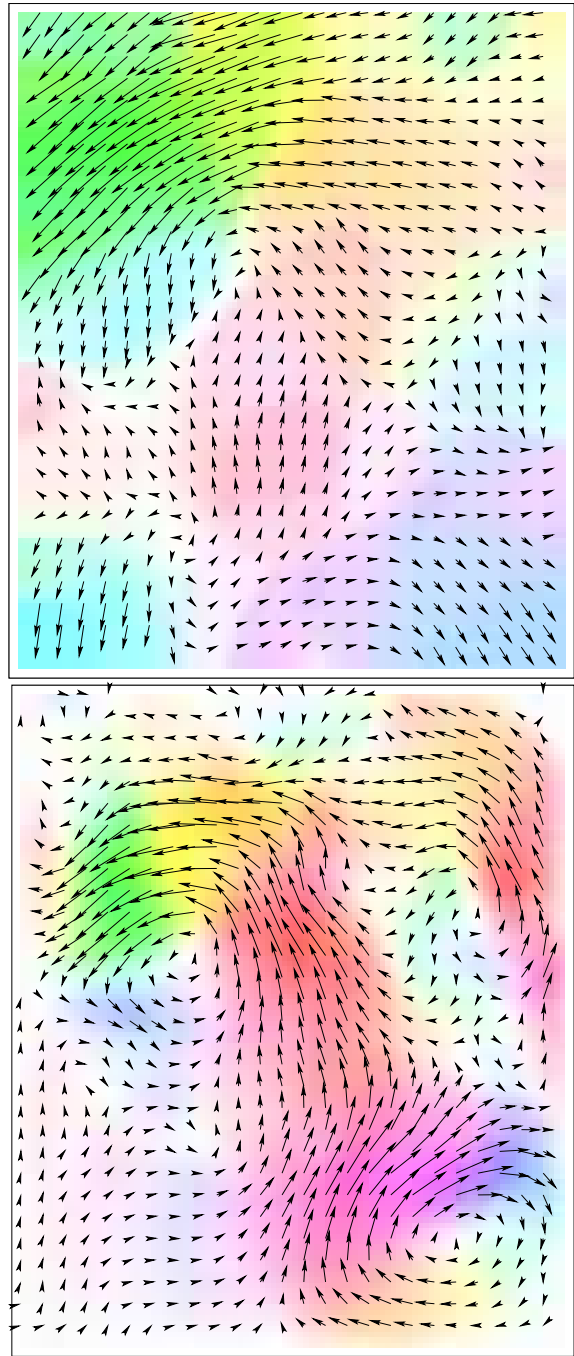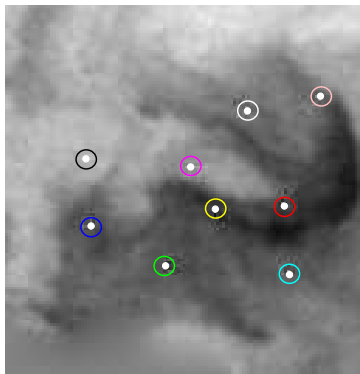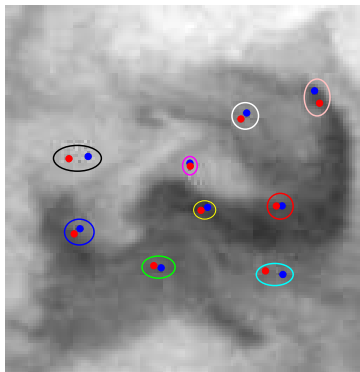
best result, while the white one means that both methods are equivalent. Again, Sun's motion results fail to track characteristic points on these data as physical processes are not correctly assessed.
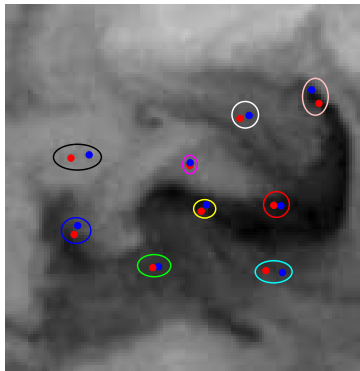
Last, EM is also compared with the optical flow estimation of Suter (Suter, 1994), that is dedicated to
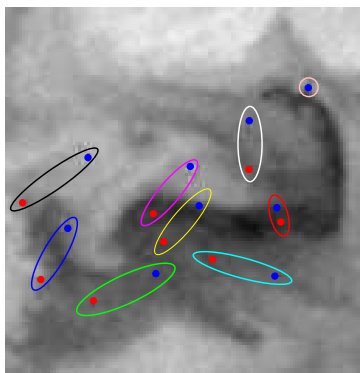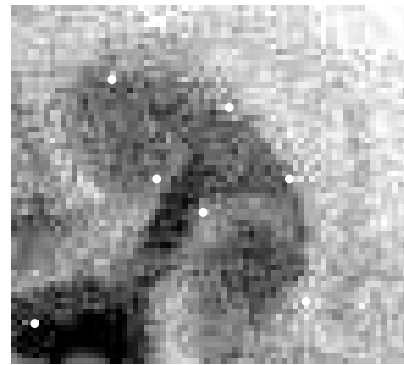
(a) Observation 1

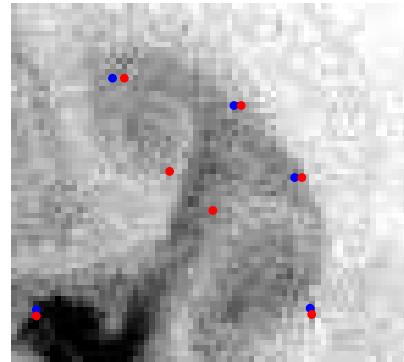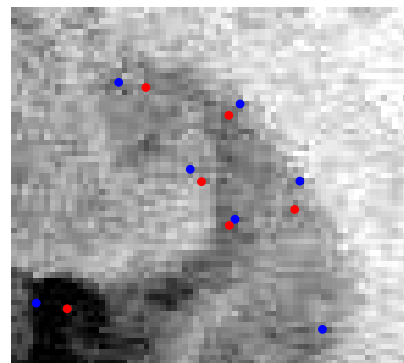(b) Observation 2

(c) Observation 3

(d) Observation 4

Figure 3: Tracking of characteristic points. Sun's algorithm in red, EM in blue.
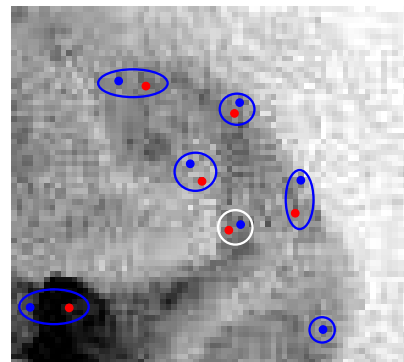
(a) Observation 1

(b) Observation 2

(c) Observation 4

(d) Observation 5

Figure 4: Tracking of characteristic points. A blue ellipse on (d) expresses that EM is the best while the white ellipse expresses that results are equivalent.

fluid flows. The SST sequence was acquired in May 14th 2005 and contains five observations at 30 min, 2 hours and 45 min, 5 hours and 15 min, 7 hours and 15 min, 16 hours and 15 min after the beginning of the studied interval. They are displayed on Figure 5. As previously, six feature points are chosen on the
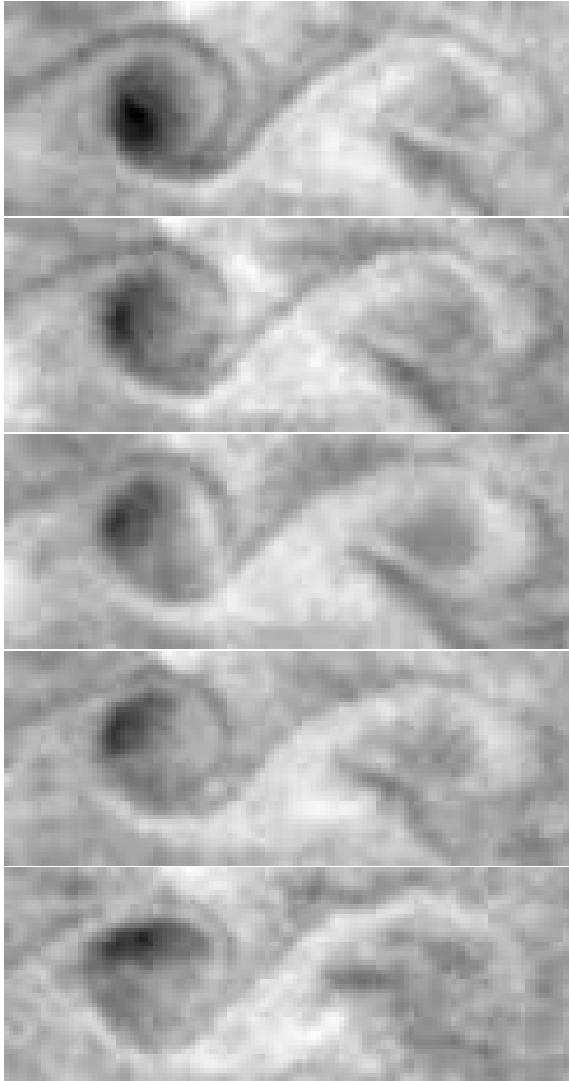

Figure 5: Five consecutive observations of the sequence acquired in May 14th 2005.

first observation and displayed on the upper image of Figure 6. Their final position on the fifth observation is given in the lower part of the same figure. Suter's and Sun's methods being based on variational optical flow approaches, they are only constrained by grey level values and not by the underlying dynamics. However, Suter's algorithm provides better result than Sun's method, because it is specifically designed for fluid flows motion. In particular, it can correctly
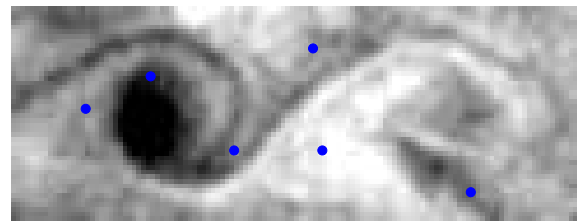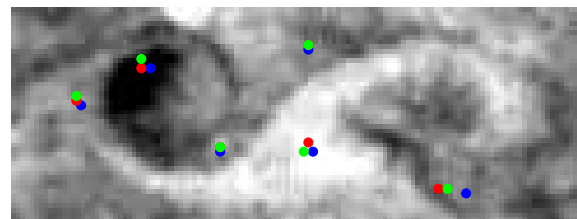

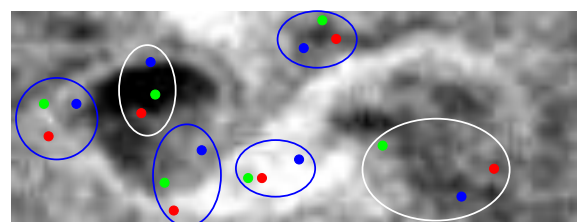(a) Characteristic points on the first observation.
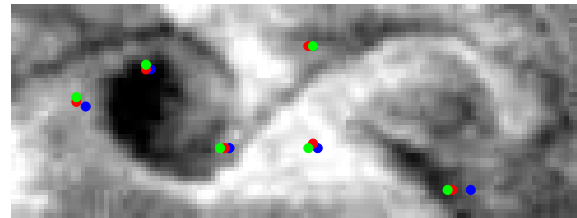
(b) On second one.
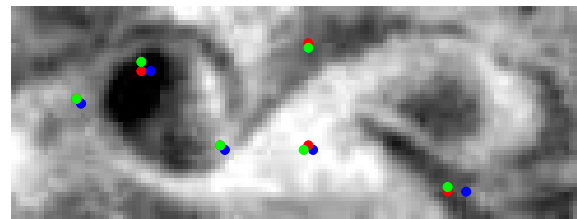
(c) On third one.

(d) On fourth one.

(e) Characteristic points on the last observation.

Figure 6: Tracking of feature points displayed in blue in (a). Sun's result is in red, Suter's in green and EM's in blue.

assess rotational motion. From left to right in Subfigure 6(e): EM gives the best result for the first, third, fourth and fifth points (blue ellipses). For the second and sixth (white ellipses) points, it is not possible to determine which one from Suter's algorithm and EM provides the best result.

The same conclusion is valid for all studied image sequences.

6 CONCLUSION

This paper describes how to learn the ocean surface dynamics from an empirical model, EM, that summarises the shallow water equations by an advection term and an additional term **a**. This last represents physical processes such as the Coriolis force, the gravity force and the viscosity. A data assimilation algorithm is defined for EM that estimates the velocity field at the first acquisition date and the additional term $\mathbf{a}(t)$ at each date of the studied interval. $\mathbf{a}(t)$ is of major importance for correctly assessing the hidden physical processes and accurately estimating motion on the whole image sequence. The algorithm does not involve any parameter other than those of the data assimilation framework (error covariance matrices). The method has been illustrated on several SST sequences of Black Sea and has been quantified by tracking feature points. Moreover, it has been compared with state-of-the-art optical flow algorithms. The conclusion is that a model of dynamics, even if simple, improves motion estimation and allows tracking of structures.

This approach may be seen as a first step to model the physical processes occurring at the ocean surface from image data. The short-term perspectives will be to compare the additional term $\mathbf{a}(t)$ with forces involved in the shallow water model, in order to further validate the ability of the empirical model to assess geophysical processes.

ACKNOWLEDGEMENTS

REFERENCES

Byrd, R. H., Lu, P., and Nocedal, J. (1995). A limited memory algorithm for bound constrained optimization. *Journal on Scientific and Statistical Computing*, 16(5):1190–1208.

Dee, D. (2005). Bias and data assimilation. *Quaterly Journal of the Royal Meteorological Society*, 131:3323–3343.

Hascoët, L. and Pascual, V. (2004). Tapenade 2.1 user's guide. Technical Report 0300, INRIA.

Hascoët, L. and Pascual, V. (2013). The Tapenade Automatic Differentiation tool: Principles, Model, and Specification. *ACM Transactions On Mathematical Software*, 39(3).

Hundsdorfer, W. and Spee, E. (1995). An efficient horizontal advection scheme for the modeling of global transport of constituents. *Monthly Weather Review*, 123(12):3,554–3,564.

Huot, E., Herlin, I., Mercier, N., and Plotnikov, E. (2010). Estimating apparent motion on satellite acquisitions with a physical dynamic model. In *International Conference on Image Processing (ICPR)*, pages 41–44.

Korotaev, G., Huot, E., Le Dimet, F.-X., Herlin, I., Stanichny, S., Solovyev, D., and Wu, L. (2008). Retrieving Ocean Surface Current by 4-D Variational Assimilation of Sea Surface Temperature Images. *Remote Sensing of Environment*, 112:1464–1475.

Le Dimet, F. and Talagrand, O. (1986). *Variational algorithms for analysis and assimilation of meteorological observations: theoretical aspects.*, pages 97–110. Tellus.

LeVeque, R. (1992). *Numerical Methods for Conservative Laws*. Lectures in Mathematics. ETH Zürich, Birkhaüser Verlag, 2nd edition.

Lions, J.-L. (1971). *Optimal Control of Systems Governed by Partial Differential Equations*. Springer-Verlag.

Oguz, T., La Violette, P., and Unluata, U. (1992). The upper layer circulation of the black sea: Its variability as inferred from hydrographic and satellite observations. *Journal of geophysical research*, 78(C8):12,569–12,584.

Papadakis, N., Corpetti, T., and Mémin, E. (2007). Dynamically consistent optical flow estimation. In *Proceedings of International Conference on Computer Vision (ICCV)*, Rio de Janeiro, Brazil.

Sasaki, Y. (1970). Some basic formalisms in numerical variational analysis. *Monthly Weather Review*, 98(12):875–883.

Sun, D., Roth, S., and Black, M. (2010). Secrets of optical flow estimation and their principles. In *Proceedings of European Conference on Computer Vision (ECCV)*, pages 2432–2439.

Suter, D. (1994). Motion estimation and vector splines. In *Proceedings of Conference on Computer Vision and Pattern Recognition (CVPR)*, pages 939–942.

Titaud, O., Vidard, A., Souopgui, I., and Le Dimet, F.-X. (2010). Assimilation of image sequences in numerical models. *Tellus A*, 62:30–47.

Trémolet, Y. (2006). Accounting for an imperfect model in 4D-Var. *Quaterly Journal of the Royal Meteorological Society*, 132(621):2483–2504.

Vallis, G. K. (2006). *Atmospheric and oceanic fluid dynamics*. Cambridge University Press. 745 pp.

Valur Hólm, E. (2008). Lectures notes on assimilation algorithms. Technical report, European Centre for Medium-Range Weather Forecasts Reading, U.K.

Wolke, R. and Knoth, O. (2000). Implicit-explicit Runge-Kutta methods applied to atmospheric chemistry-transport modelling. *Environmental Modelling and Software*, 15:711–719.